Effect of system composition on mixing in binary fluidised beds

Werner, D.; Davison, H.; Robinson, Ellis Shipley; Sykes, J.A.; Seville, J.P.K.; Wellings, A.; Bhattacharya, S.; Sanchez monsalve, D.A.; Kokalova wheldon, Tz.; Windows-Yule, C.R.K.

DOI:
10.1016/j.ces.2023.118562

Chemical Engineering Science 271 (2023) 118562

Contents lists available at ScienceDirect

Chemical Engineering Science

journal homepage: www.elsevier.com/locate/ces

Effect of system composition on mixing in binary fluidised beds

D. Werner [a,*], H. Davison [a], E. Robinson [a], J.A. Sykes [b,a], J.P.K. Seville [a], A. Wellings [c], S. Bhattacharya [c], D.A. Sanchez Monsalve [c], Tz. Kokalova Wheldon [b], C.R.K. Windows-Yule [a]

[a] School of Chemical Engineering, the University of Birmingham, Edgbaston, Birmingham B15 2TT, UK
[b] School of Physics and Astronomy, the University of Birmingham, Edgbaston, Birmingham B15 2TT, UK
[c] Recycling Technologies Ltd., Unit B2, Stirling Court, Stirling Rd, Swindon SN3 4TQ, UK

GRAPHICAL ABSTRACT

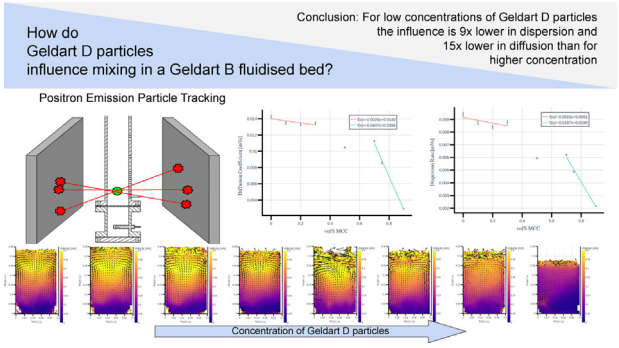

ARTICLE INFO

Article history:
Received 5 October 2022
Received in revised form 23 January 2023
Accepted 8 February 2023
Available online 13 February 2023

Keywords:
Positron emission particle tracking
Fluidised bed
Mixing

ABSTRACT

The influence of bed composition – that is, the relative proportions of different components – on the mixing of fluidised beds containing mixtures of Geldart group B and D particles is of considerable importance to a variety of contemporary industrial processes, such as plastic recycling and biomass gasification. In this study, we use Positron Emission Particle Tracking (PEPT) to analyse the detailed, three-dimensional flow dynamics of such a system and, from these measurements, determine the rate of mixing as a function of bed composition. Our results show that for comparatively small fractions ($\phi_D \lesssim 30\%$) of Group D particles, the system's mixing dynamics are only weakly affected by variations in ϕ_D. For higher concentrations, however, the mixing effectiveness of the system is observed to decrease sharply, and marked changes in the system's flow patterns are observed, with a previously undocumented metastable state recorded for the highest concentrations of group D particles.

1. Introduction

The mixing of materials in fluidised beds is crucial to a number of processes spanning multiple industrial sectors (Kunii and Levenspiel, 1991; Nienow et al., 1997; Formisani and Girimonte, 2003). The dynamics of solid mixing of Geldart B/D mixtures is of direct importance to various processes, notably combustion, gasification and pyrolysis (Salatino and Solimene, 2017); one application of particular contemporary importance is in the pyrolysis-based recycling of plastic waste (Edel, 2021). In the case of plastics recycling company Recycling Technologies, a fluidised bed of heated sand particles is used to pyrolyse coarsely-shredded waste plastics, producing virgin-quality plastic feedstocks and clean, low-sulphur fuels (Griffiths, 2020; Gear et al., 2018). In order to produce high-quality end products, however, the achievement of uniform tem-

* Corresponding author.
E-mail address: dxw963@bham.ac.uk (D. Werner).

https://doi.org/10.1016/j.ces.2023.118562
0009-2509/

perature, which demands fast, effective mixing, is of paramount importance. It is generally accepted, and has been repeatedly demonstrated experimentally, that increasing the fines fraction in binary or ternary fluidised beds acts to decrease the minimum fluidisation velocity, u_{mf}, thereof (Jena et al., 2008; Taib and Kumoro, 2003). It is similarly well-known (Kim et al., 2013) that when the gas velocity exceeds the minimum fluidisation velocity, U^f_{mf}, of the fine component of a fluidised bed but falls below that of the coarse component, U^c_{mf}, segregation is liable to occur. Currently less well-understood, however, is the specific relationship between concentration and the *rate* of mixing.

Earlier research on fluidisation of mixtures of particles (Geldart, 1986; Nienow et al., 1978; Rowe and Nienow, 1976) concentrated on establishing whether a mixture of two types of particles of given properties would segregate when fluidised and on how this is affected by the fluidising velocity. In general, particle density was found to be more important than size in promoting segregation. Approximate rules of behaviour were established, including predictions for the mixing index M_I, defined as the concentration of the material of interest at some level in the bed divided by its average concentration. Work was also done of establishing the multiple mechanisms of segregation and how this is related to bubble motion in the bed. Related work has considered the effects of bed shape on segregation (Gernon and Gilbertson, 2012) and described the occurrence of segregation bands and other structures given a specific flow velocity (Gilbertson and Eames, 2001).

More recently, a number of studies have used numerical modelling tools, namely computational fluid dynamics and discrete element method, to study the same phenomena, reinforcing the observations of the earlier experimental studies. Hameed et al. (2019), Oschmann et al. (2014), Huilin et al. (2003),Bokkers et al. (2004).

Much less work has been done on the dynamics of segregation (Nienow and NS, 1980; Chiba, 1986). Leaper et al. (2004) measured the rate of segregation in a system of two group B particles by monitoring the position of the interface between the separated layers, and showed that the local concentration x of the coarse (“jetsam”) fraction approached an equilibrium value x_∞ according to a first-order equation of the form

$$x - x_\infty = (x_0 - x_\infty)e^{-\omega_c t} \tag{1}$$

where ω_c is a rate constant. Olaofe et al. (2013) investigated the dynamic mixing of Geldart D particles in a pseudo-two-dimensional fluidised beds using digital image analysis. They found that binary systems could segregate slightly at fluidisation velocities just exceeding the incipient velocities of all the individual components, while the ternary mixture becomes well mixed at velocities even well below the incipient velocity of the largest particles.

As in other aspects of fluidisation, experimental investigation is hampered by the opaque nature of the system, so that studies have predominantly concentrated on external measures such as overall and local pressure measurements (Olivieri et al., 2004), direct observations at the wall (Bai et al., 2022) or frozen bed methods (Nienow et al., 1987; Wu and Baeyens, 1998).

In the present work, we utilise positron emission particle tracking (PEPT), a non-invasive, three-dimensional imaging technique, to asses the mixing dynamics of group B and D particles across the range of relative concentrations.

2. Materials and Methods

2.1. Materials

We explore a cylindrical, gas-fluidised bed of inner diameter 94 mm, as depicted in Fig. 1, containing a binary mixture comprising near-spherical silica sand (Geldart group B) and Microcrystalline cellulose (MCC Geldart group D) particles with a bed height to diameter ratio $\frac{H}{D} = 2$. Table 1 The particle size distributions for both of these materials are specifically chosen to be directly representative of those used in the waste plastic recycling applications discussed in Section 1, with MCC acting as a surrogate for the waste plastic component due to its comparatively greater ability to hold β^+ radioactivity (see Section 2.2). The particle size distributions of the bed materials, measured using a Sympatec QicPic, are shown in Fig. 2. The volume fraction ϕ_D of the Geldart group D material is varied in the range $0 \leqslant \phi_D \leqslant 90\%$, corresponding to mass fractions detailed in Table 2.

The bed is fluidised using room temperature air through a perforated plate distributor with twelve 1.2 mm orifices on a 20.5 mm square pitch, the flow rate controlled by calibrated rotameters. For each value of ϕ_D tested, the minimum fluidisation velocity is determined via standard pressure-drop measurements; calculated values of the U_{mf} can be seen in Section 3.1. PEPT measurements were then conducted for each ϕ_D at a constant multiple of the measured incipient velocity, $U = 3U_{mf}$, a value chosen to be representative of the flow rates used in the aforementioned waste-plastic pyrolysis systems.

2.2. Data acquisition: positron emission particle tracking

Positron emission particle tracking (PEPT) is a technique which allows the fully three-dimensional trajectories of one or more radioactively-labelled ‘tracer particles’ to be recorded with high temporal and spatial resolution, even as they move through the interior of dense, optically opaque systems, such as those explored here (Parker et al., 2002; Windows-Yule et al., 2020; Windows-Yule et al., 2021). Other than being labelled with a positron-emitting radioisotope, the tracers used are typically physically identical to others of the same species in the system, making PEPT a truly non-invasive technique. Though not necessary to the comprehension of the current work, the interested reader may find further details regarding PEPT, its underlying algorithms, and the radiolabelling of tracer particles in reference (Windows-Yule et al., 2022).

One of the great benefits of PEPT in the present application is that – unlike purely Eulerian methods such as electrical capacitance tomography (ECT)(Zhang et al., 2014; Wang and Yang, 2020) which are commonly used to investigate fluidised beds – PEPT can extract both Eulerian *and Lagrangian* information, allowing both the macroscopic (bulk) and microscopic (particle-level) mixing *dynamics* of the systems of interest to be directly explored. The spatial resolution of PEPT is also significantly higher than that of electrical capacitance tomography (Windows-Yule et al., 2022).

In the present study, we track exclusively the Geldart D component of our system. While it is possible to use PEPT to reconstruct the time-averaged, steady-state mixing/segregation patterns and mixing indices of fluidised beds and other systems (Windows-Yule et al., 2020), in the present work we consider only the mixing *rates* of the Geldart D component of our system. This is due to the fact that our study aims to inform applications such as waste plastic pyrolysis and biomass gasification, whereby the plastic/biomass represented by our group D particles will devolatilise long before a steady segregation pattern may be achieved. As such, we focus instead on dynamic quantities, namely the dispersion and diffusion rate of the group D particles.

In the following subsections, we detail the ways in which the key fields and quantities of interest to this study are extracted from raw PEPT data.

2.2.1. Characterising flow patterns

The flow patterns exhibited by a a fluidised bed are instrumental in determining the quality of mixing achieved (Windows-Yule

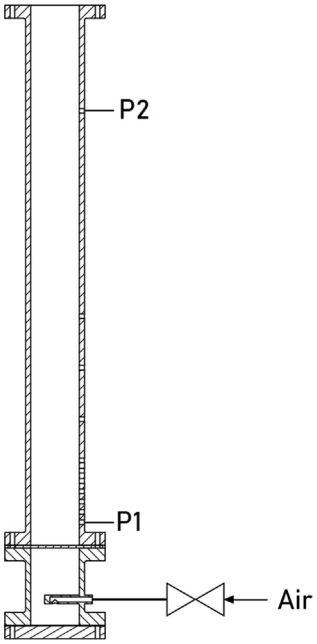

Fig. 1. Schematic of the experimental setup, consisting of one 94 mm fluidised bed with a height of 1 m. Pressure drops were measured using the difference between P1 and P2.

Table 1
Material properties of the Microcrystalline cellulose and silica sand used in the PEPT experiments.

	MCC	Sand
Density ρ[kgm^{-3}]	1460	2800
Sphericity ϕ [–]	0.940	0.917
$\bar{d}$ [μm]	1200	320
d10 [μm]	1040	200
d90 [μm]	1250	400

et al., 2020), and more generally in understanding the bed dynamics. PEPT facilitates the direct visualisation of flow fields within a system in one-, two- or three-dimensional space. We consider in this work the case of a two-dimensional, depth-averaged projection, which captures the main qualitative features of the flow whilst also maintaining good statistics. This Cartesian representation is chosen over an azimuthally-averaged cylindrical polar representation due to the fact that the flow patterns produced in some cases (notably those with high loadings of Group D particles) do not exhibit the axisymmetry typically observed in fluidised beds.

The pseudo-instantaneous velocity, $\vec{v}_i$ of a PEPT tracer at a given point in time, t_i, can be determined simply using a central difference approach, i.e.

$$\vec{v}_i = \frac{\vec{r}_{i+j} - \vec{r}_{i-j}}{t_{i+j} - t_{i-j}} \tag{2}$$

To determine the optimal value of j, we use Eq. 2 to calculate the velocity with various different values of j. We then calculate the velocity vector-field as outlined in Section 2.2 and compare it to a base field. We compute the vector difference of each vector in each cell with:

$$\delta v_i = \sqrt{\left(v^b_{i,x} - v^w_{i,x}\right)^2 + \left(v^b_{i,y} - v^w_{i,y}\right)^2} \tag{3}$$

where the first and second suffixes "i" and "x/y" represent the cell index and the dimension, respectively. Then we express the difference as the mean difference across the entire field calculated with Eq. 4.

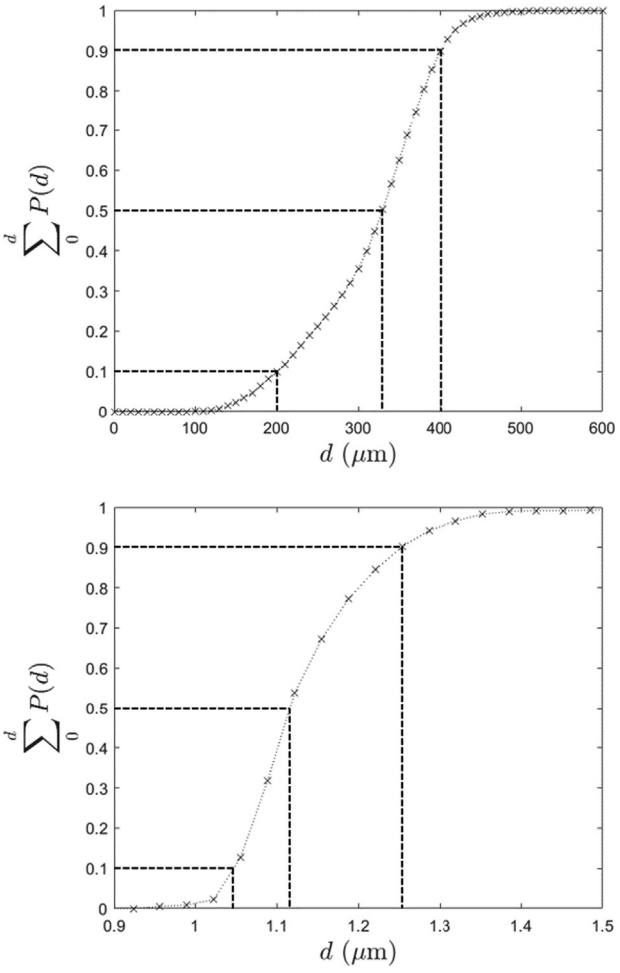

Fig. 2. Cumulative particle size distribution for the silica sand (above) and MCC (below) particles used in experiment.

Table 2
Mass of MCC and silica sand used in PEPT experiments for different volume percentages.

Vol % MCC	Mass MCC [g]	Mass Sand [g]
0	0	2400
10	120	2160
20	240	1920
30	360	1680
50	600	1200
70	840	720
75	900	600
90	1080	240

$$\overline{\Delta v} = \frac{\sum_{i=0}^{N} \delta v_i}{N} \tag{4}$$

where N is the total number of cells in the vector-field. Fig. 3 shows the resulting error graph for a j value between 1 – 7 with a base field taken as j = 3. The graph shows clearly that the difference between j = 2 and the base line is non-negligible, whereas j = 4 and the baseline at j = 3 do not show significant difference with an overall difference of only 3.4mm/s[1]. We select $j = 3$ as the optimal value because larger values do not significantly affect the results

[1] The deviation for small j is to be expected as at these short timescales the measurement no longer averages out the random motion of the particle (Windows-Yule et al., 2022).

and a smaller value is preferred due to the loss of information resulting from averaging. Once the velocity has been calculated for all data points acquired, the experimental volume is subdivided into a grid of two-dimensional 'pixels' in the plane of interest, here the *x-z* (horizontal-vertical) plane, such that any convection rolls within the system may be visualised. The mean velocity for each pixel can then be determined by summing the velocities of all particle locations falling within its bounds, and dividing by the total number of locations in said pixel (Wildman et al., 2000; Windows-Yule et al., 2022).

An example of a velocity vector field created using the methodology described above can be seen in Fig. 4. In this figure, the direction of the arrow represents the mean direction of flow in the plane of interest, while its length represents the velocity magnitude through a given point in space. In the image shown, one can clearly distinguish, in the upper part of the bed, the two-roll flow pattern commonly associated with bubbling fluidised beds with solids flow up in the centre, carried by the bubbles, and down at the walls. (Geldart, 1986).

2.2.2. Characterising micro- and macro-mixing

There are several ways in which the degree of mixing within a fluidised bed can be quantified using PEPT. For example, the steady-state distribution of one (Windows-Yule et al., 2020) or both (Windows-Yule et al., 2014) components throughout the system can be measured. For applications such as waste-plastic pyrolysis, however, we are less interested in the final, steady-state distribution of materials and more interested in the *rate at which* the material to be decomposed is likely to be distributed throughout the system, as this will determine the uniformity of the process. When considering the distribution of the group D material through the bed, we must consider both macro-mixing and micro-mixing (Villermaux, 1986).

To quantify the former property, we use PEPT to measure the mean squared displacement, and thus a granular analogue to the diffusion coefficient, of the group D particles, which tells us how rapidly a typical particle will diverge from its initial position within the system.

In order to measure the mean squared displacement of the tracer over a period $\Delta t = t - t_0$, we begin by dividing the measured particle trajectory into a series of overlapping segments or 'time windows', each of length Δt. For a single such segment starting at time t_0^i, the squared displacement of the tracer can be written as:

$$\Delta r_i(t_0^i, \Delta t)^2 = |\vec{r}(t_0^i + \Delta t) - \vec{r}(t_0^i)|^2. \tag{5}$$

Under the ergodic assumption (Wildman et al., 2000), the average over all time can be taken as equivalent to an ensemble average over all particles of the same species as the tracer, meaning that the mean squared displacement (MSD) can be computed as:

$$\begin{aligned} \mathrm{MSD}(\Delta t) &= \left\langle |\vec{r}(t_0 + \Delta t) - \vec{r}(t_0)|^2 \right\rangle \\ &= \tfrac{1}{N_{seg.}} \sum_{i=1}^{N_{seg.}} \Delta r_i(t_0^i, \Delta t)^2 \end{aligned} \tag{6}$$

where $N_{seg.}$ is the total number of time segments into which the particle trajectory has been separated.

From here, the self-diffusion coefficient of the particle species of interest can then be determined from the Einstein relation:

$$D = \lim_{t \to \infty} \frac{1}{2\mathscr{D}t} \left\langle |\vec{r}(t) - \vec{r}(t_0)|^2 \right\rangle \tag{7}$$

where $\mathscr{D}$ is the dimensionality of the system; in our case $\mathscr{D} = 3$, as the tracer is free to explore all three spatial dimensions, however, due to the geometrical restrictions of the systems, the MSD will approach a maximum value depending on the traversable volume of the system. To avoid this influence we calculate the diffusion coefficient as the gradient in the linear regime of the MSD, determined by the minimum R value of a first order least square fit with 10 data points.

The value of the diffusion coefficient provides a useful quantitative measure of the rate at which the particles move through the system as a whole; it does not, however, offer any information regarding how quickly a given Group D particle will separate from

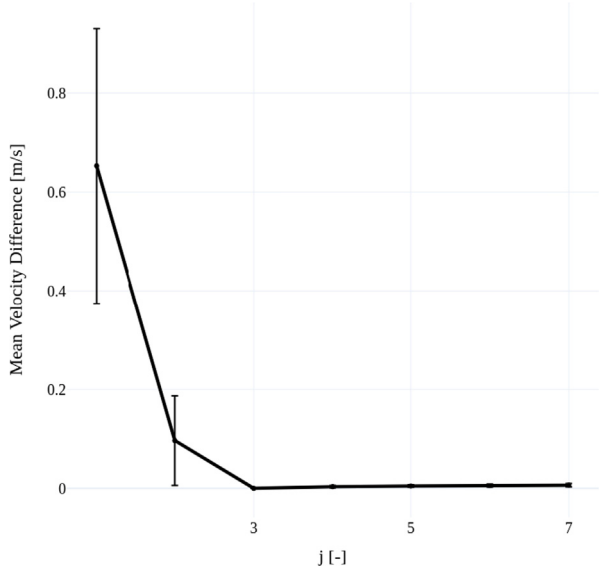

Fig. 3. The mean difference of the velocity vector field with change in parameter j.

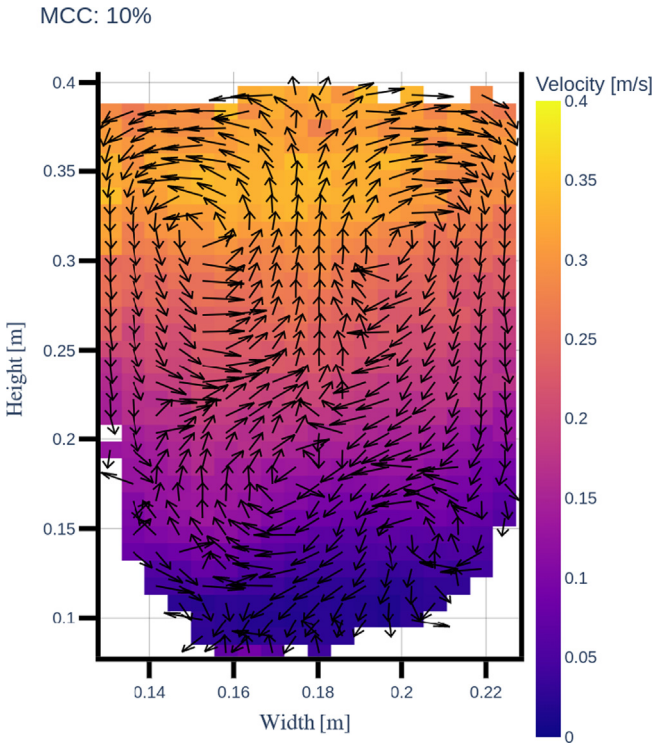

Fig. 4. Example of a velocity vector field extracted from PEPT data with underlying velocity Investigating the dynamics of segregation of high jetsam binary batch fluidised bed systemsmagnitude field. For ease of interpretation, the lengths of the arrows are kept uniform, with the magnitude of the velocity indicated instead by the colour scale shown.

other, neighbouring particles – i.e. it provides insight into the rate of *macro-mixing* within the system, but offers little information regarding *micro-mixing*.

To quantify the rate at which micro-mixing occurs within the system, we consider the *dispersion* (Martin et al., 2007; Seville et al., 2005) of particles. In order to do so, we first subdivide the experimental volume into a series of three-dimensional voxels. For a given voxel containing N particle locations, each location falling within said voxel is considered as the starting point of a separate trace. Each trace is then followed over a user-defined period of time, t, and the new positions, $\vec{r}_i$, of each tracer at time t are recorded (see Fig. 5). The dispersion can then be simply calculated as the variance of these final positions, i.e.

$$\sigma^2 = \frac{1}{N}\sum_{i=1}^{N}(\vec{r}_i - \langle\vec{r}\rangle)^2 \tag{8}$$

where $\langle\vec{r}\rangle$ is the average over all final positions. Clearly, if all particle trajectories beginning in the aforementioned voxel remain tightly grouped together (i.e. they travel as a single 'packet' of material, as illustrated in Fig. 5(b)) $\sigma^2 \to 0$. Conversely, if particles rapidly spread out from one another (as illustrated in Fig. 5(a)) σ^2 will quickly achieve a large value. As such, the dispersion provides a clear quantification of the expected degree of micro-mixing within a given region of the system. The characteristic dispersion across the system as a whole – referred to as the 'mixer effectiveness' (Martin et al., 2007; Seville et al., 2005) – can then be obtained by averaging over all voxels within the system.

In order to obtain a quantity approximately equivalent to the diffusion coefficient for dispersive mixing, we plot the whole-system dispersion as a function of time, and determine the region of this plot for which the dispersion increases linearly with time, i.e. the period during which free dispersion is occurring, and particle motion has not begun to be limited by the system size (Windows-Yule and Parker, 2014) (see Fig. 6). Similarly to the case of diffusion, the desired linear region is determined by finding the region of the dispersion vs. time plots for which a first-order linear least squares fit spanning at least 10 data points yields the minimum R^2 value for each trace. We then simply find the gradient of this linear region, which represents the characteristic 'dispersion rate' of the system as a whole.

2.2.3. Bubble analysis

Though PEPT cannot directly image the motion of bubbles, the technique can nonetheless be used to infer certain key characteristics relating to bubble motion. Bubbles carry solids with them in their wakes, the amount of which depends on their size and the bed material. Particles in these wake regions can be used to indirectly characterise the velocity and frequency of bubbles occurring. The vertical trajectory of a particle in a bubbling fluidised bed is shown in Fig. 7. These trajectories typically consist of alternating periods of slow descent and rapid rise, the latter corresponding

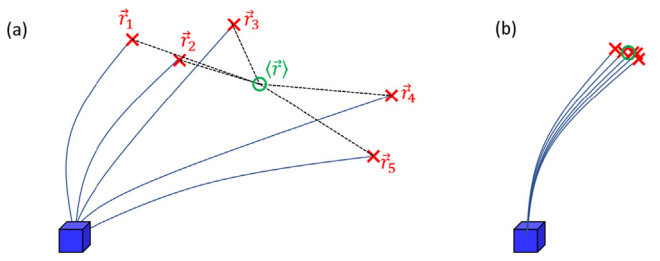

Fig. 5. Schematic diagram illustrating (a) a case in which the particles from a given voxel experience strong dispersion and (b) a case in which little dispersion is observed.

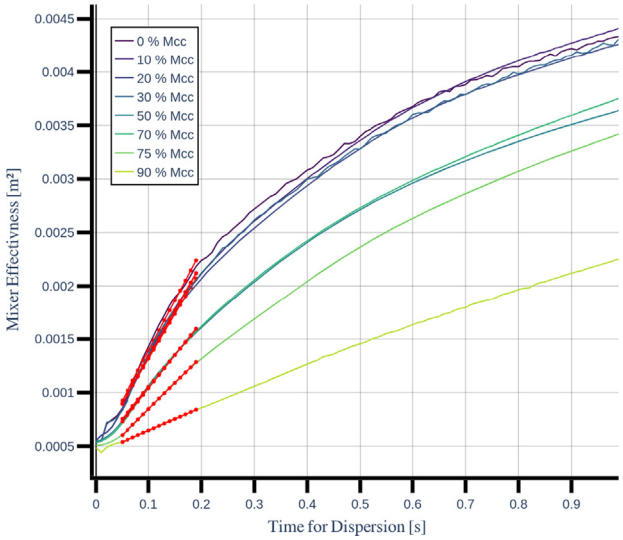

Fig. 6. Mixer effectiveness for different MCC loadings as a function of time. All curves demonstrate the typical form expected (Martin et al., 2007), initially increasing in a linear manner, before tending towards an asygmptote due to the finite size of the vessel. Red lines indicate first order least squares fits in the linear region, used to calculate the dispersion rate.

to the situation in which the particle is inside the wake or drift of a bubble. To isolate these periods, typically referred to as 'jumps' (Stein et al., 2000) (that is, to determine when a particle is being 'carried' by a bubble), a set of three criteria must be fulfilled (Stein et al., 2000):

I. The particle must be travelling upward.
II. The particle's vertical velocity must exceed a given threshold, v_{thresh}, as bubbles (and particles entrained thereby) are expected to travel more rapidly than material in the emulsion phase.
III. The upward motion must persist across a suitably large range of space and time that it cannot simply be attributed to statistical error or random motion.

In the present work we take $v_{thresh} = 0.1\text{m/s}$ and specify that the particle must have travelled at least 2.4 centimetres in order for a given section of the tracer's trajectory to be considered a 'jump'. These values were implemented in previous work by Stein et al. (Stein et al., 2000) and are expected to be similarly suitable for the geometry and conditions explored here.

3. Results

3.1. Preliminary results – Minimum fluidisation velocities

Before conducting the PEPT measurements, it was first necessary to determine the minimum fluidisation velocity for the various relative concentrations of Geldart group B and D particles explored. Our experimental measurements are shown in Fig. 8, showing a general decrease in the minimum fluidisation velocity with an increasing fraction of fines (here the group B sand particles), as expected from prior literature (Taib and Kumoro, 2003; Jena et al., 2008). Indeed, our work shows quantitative agreement with the correlation of Chiba et al. (Chiba et al., 1979):

$$u_{mf} = \frac{u_{mf}^F}{\left(1 - \frac{u_{mf}^F}{u_{mf}^C}\right)x^F + \frac{u_{mf}^F}{u_{mf}^C}}, \tag{9}$$

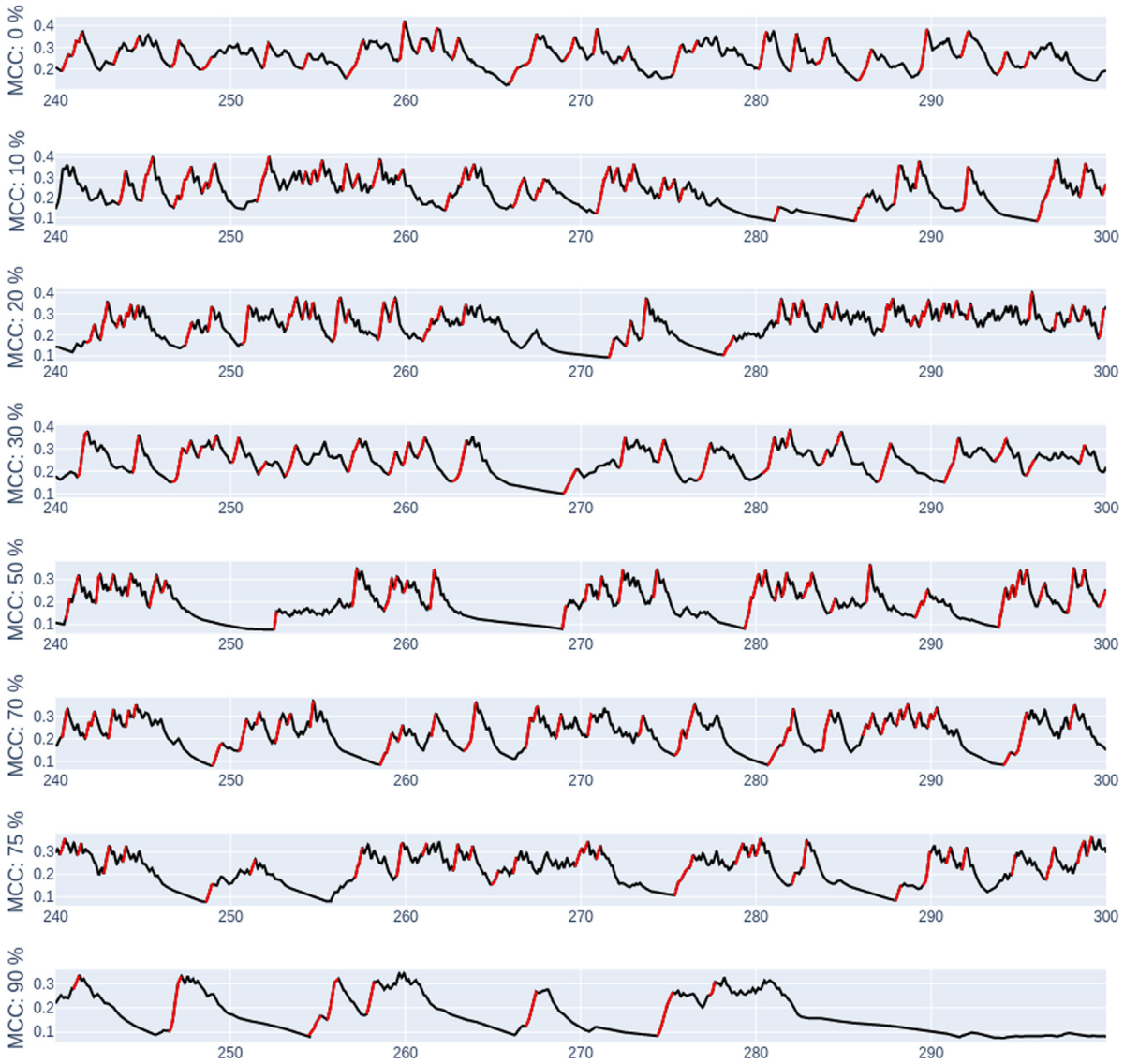

Fig. 7. Vertical particle position over time for MCC concentrations ranging from 0 to 90 *vol.%*. Red markings indicate jumps in which the particle is trapped inside a bubble.

where the subscripts *F* and *C* correspond, respectively, to the fine, more easily-fludised (sand) component and the coarse, harder-to-fluidise (MCC) component.

3.2. Macro-mixing

Fig. 9 shows values of the diffusion coefficient, *D*, calculated in the manner described in Section 2.2.2, for various volumetric concentrations of MCC. The voxel elements in this calculation have a size of 1cm in each dimension, corresponding to 1600 voxel-elements in the system. The region valid for the calculation of the dispersion coefficient lies between 0.05s and 0.2*s* and the particles in this region can be expected to travel between 0.01m and 0.04m within this timeframe. In all cases shown, the bed is fluidised with a gas flow rate $U = 3U_{mf}$, calculated based on the data in the preceding subsection.

Firstly notable from Fig. 9 is that there exists a clear, general trend of decreasing *D* with increasing MCC concentration – in other words, the diffusion of group D particles through the system is observed to slow as the concentration thereof increases. Upon closer inspection, our results also suggest the existence of two distinct

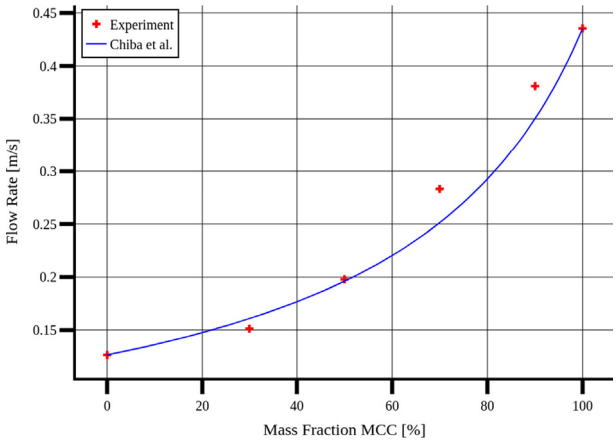

Fig. 8. Variation of the minimum fluidisation velocity, U_{mf}, with system composition – specifically the volume fraction of MCC particles. The dashed line represents a fit according to the correlation of Chiba et al. (Chiba et al., 1979). Error bars correspond to the standard deviation observed across 5 repeat measurements.

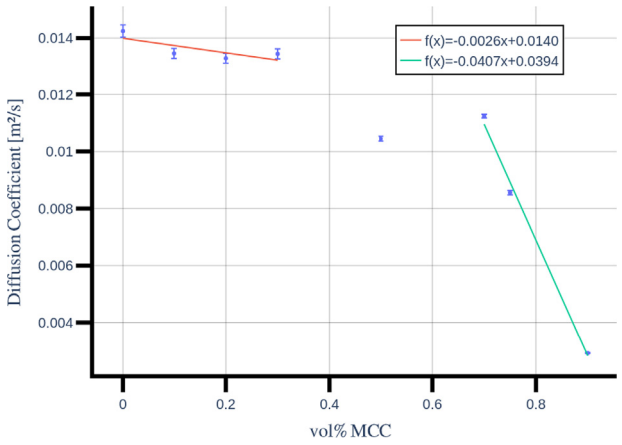

Fig. 9. PEPT-measured diffusion coefficient for systems possessing differing volumetric concentrations of Group D (MCC) particles. Error bars correspond to the RMSE of the first-order least squares fit from which the diffusion coefficient is calculated.

regimes: for comparatively low concentrations ($\phi_D \lesssim 40\%$) of group D particles, the trend is relatively shallow suggesting that the addition of coarse particles does not significantly impact the rate of mixing within the system. For higher concentrations ($\phi_D \gtrsim 60\%$), however, the inclusion of a higher volume fraction of coarse particles is observed to induce a sharp decrease in the diffusion coefficient, indicating a dramatic reduction in the rate of macro-mixing within the system. It is worth reiterating here that this marked decrease in the mixing rate of the group D material occurs in spite of a *significant increase* in the absolute gas flow rate through the system so as to maintain a constant $U = 3U_{mf}$ for all systems, making these findings all the more striking.

3.3. Micro-mixing

Fig. 10 shows values of the dispersion rate (see Section 2.2.2) for various volumetric concentrations of MCC. As previously, the bed is fluidised with a gas flow rate $U = 3U_{mf}$ in all cases.

The general trends observed in Fig. 10 are broadly similar to those shown in Fig. 9 – in other words, the concentration of group D particles within the system has a similar influence on both micro- and macro-mixing. To put it differently, increasing the concentration of group D particles acts to inhibit both the motion of said particles through the system, as well as their motion relative to one another.

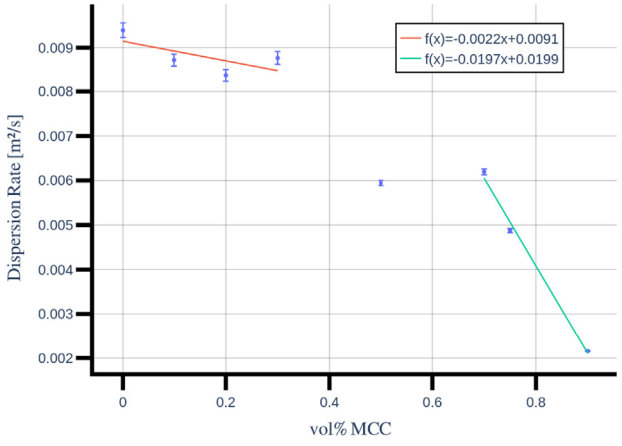

Fig. 10. PEPT-measured dispersion rate (see Section 2.2.2) for systems possessing differing volumetric concentrations of Group D (MCC) particles. Error bars correspond to the RMSE of the first-order least squares fit from which the dispersion rate is calculated.

3.4. Flow patterns

Fig. 11 shows PEPT-measured velocity vector fields illustrating the flow patterns and velocity magnitudes observed for the various concentrations, ϕ_D, of group D particles explored in our experiments. From this figure, we can clearly see the system's flow patterns change as the ratio of group D to group B particles increases, even as all other relevant variables are held constant. The velocity of the particles also decreases, the difference being particularly pronounced for higher concentrations of group D particles.

For low concentrations of group D particles ($\phi_D \in [0\%, 20\%]$) we can distinguish two distinct convection rolls within the system. For moderate concentrations ($\phi_D \in [50\% - 75\%]$) the symmetry of the rolls in the upper part of the bed becomes broken, indicating increasingly chaotic behaviour in the bed, with the spatial and temporal distributions of bubbles within the bed become less consistent. Perhaps most strikingly of all, for the highest concentration tested ($\phi_D = 90\%$), the flow pattern is observed to be *metastable* – that is to say the (typically single) convection roll observed will spontaneously change direction at seemingly random intervals in time; the image shown in the bottom-right panel of Fig. 11 represents a temporal average of this metastable flow.

3.5. Bubble behaviour

As introduced in Section 2.2.3, mixing in fluidised beds is driven by bubbles, which carry solids with them as they rise up the bed. Bubble coalescence and splitting enhance solids exchange between rising bubbles and the dense phase around them so that particles may attach or detach from bubbles at any point in their travel. Nevertheless, overall circulation can easily be detected. In beds of wide size distribution or several particle types, as here, the behaviour is complicated by preferential attachment and/or detachment of particles to and from bubbles. Fig. 7 shows the PEPT vertical position of the larger component (MCC) over time for a series of different concentrations of that component, which typically show rapid upward movement near the centre and slower downward movement near the wall. It is immediately apparent that the frequency of circulation is strongly affected by the bed composition, reducing with higher concentration of the larger component, as expected. In general, circulation rate is proportional to excess gas velocity (Geldart, 1986) which reduces as the proportion of the larger component increases, because the effective minimum fluidisation velocity increases. It has also been shown (Geldart, 1986) that bubble shape is affected by particle size such that the wake volume becomes smaller relative to the bubble volume as the particle size increases. This means that bubbles carry less bed material for a given excess gas flow. The combination of these two effects causes a marked decrease in the activity of the bed, which is indicated by the particle specific bubble frequency presented in 12.

4. Discussion and Conclusions

In the preceding sections we have seen that, for binary mixtures of Geldart group B and D materials, increasing the relative concentration, ϕ_D, of the coarser group D particles causes a general decrease in the rate of both micro- and macro-mixing, even as the absolute gas flow velocity through the system is increased. In both cases, two distinct regimes are observed – a gentle decrease

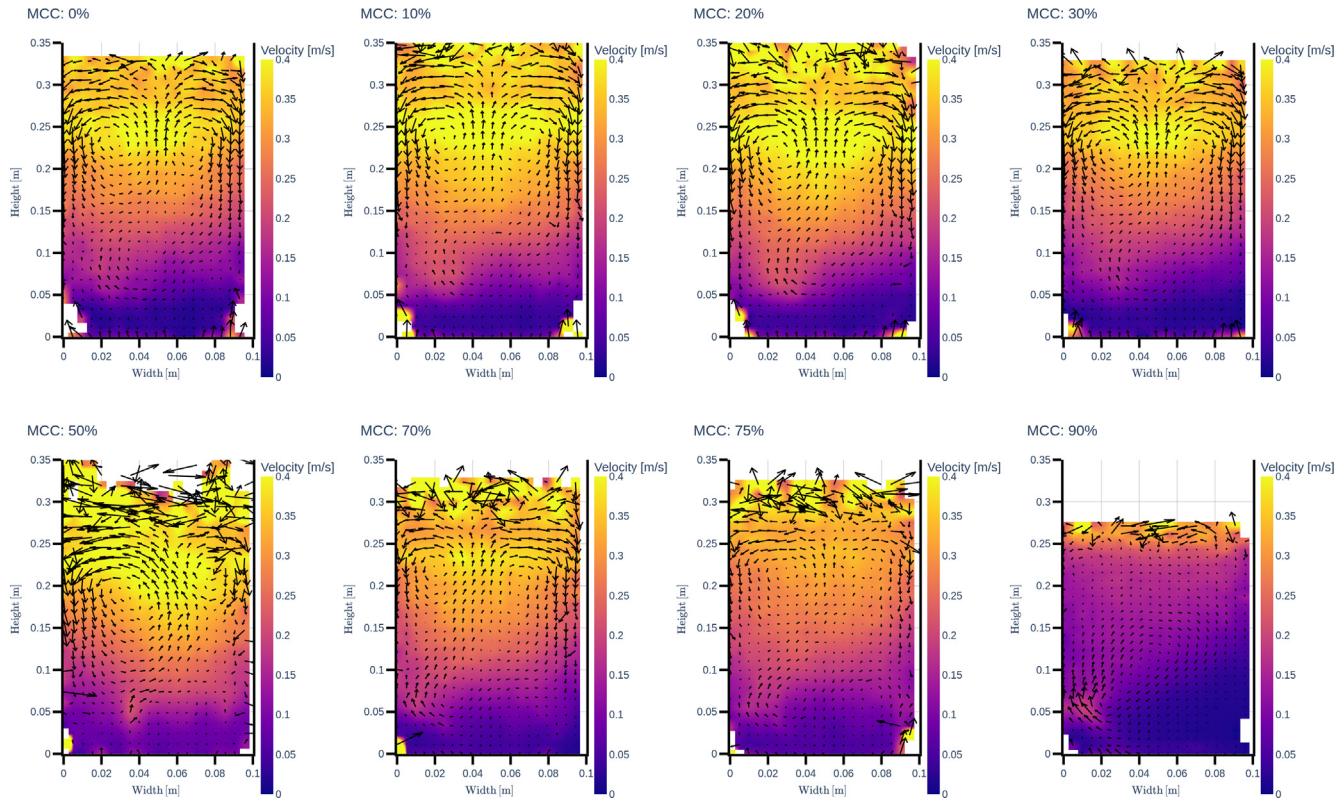

Fig. 11. Two-dimensional, depth-averaged velocity vector fields for systems comprising differing volumetric concentrations (ϕ_D) of Geldart group D particles.

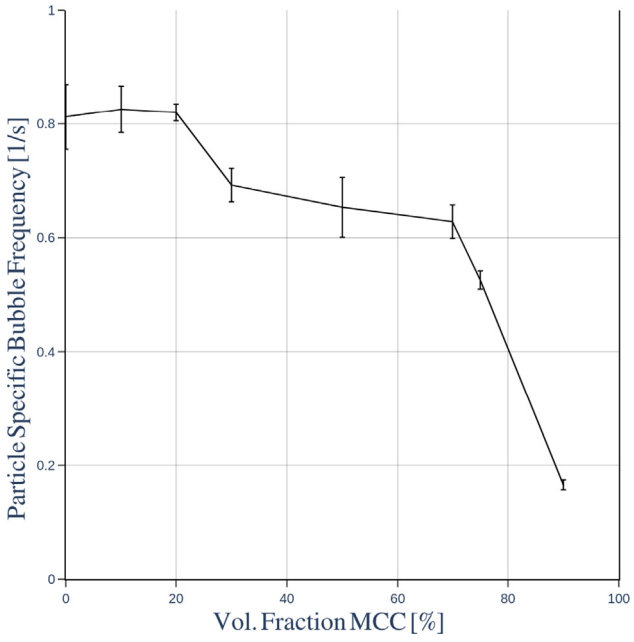

Fig. 12. Extracted mean particle specific bubble frequency for a 94 mm fluidised bed at a flow rate of three times the minimum fluidisation velocity for different volume fractions of MCC. Line shown as a guide to the eye.

in mixing rate with ϕ_D for low ϕ_D, and a sharper decrease for high ϕ_D. Increasing ϕ_D is also observed to precipitate a transition from a two-roll flow pattern at low ϕ_D to a one-roll pattern at high ϕ_D. Interestingly, the transition point between the two mixing regimes mentioned above seemingly aligns with the transition from a multiple-roll to a single-roll flow pattern.

The observation of a clear correlation between the observed mixing rates and flow patterns agrees well with prior research (Laverman et al., 2012; Stein et al., 2000), which suggests that quadruple- and single-roll patterns are, respectively, the most and least conducive to mixing. The observed changes in flow regime cannot entirely explain our results, however, as even within each regime we still observe a general decrease in mixing rate with increasing ϕ_D. This general decrease can perhaps be explained as an increase in the effective viscosity (Lun et al., 1984) of the system with an increasing proportion of larger particles, which will naturally inhibit both the micro- and macro-mixing of particles.

Overall, our findings indicate that for applications such as waste plastic pyrolysis, where rapid mixing of group B and D particles is required, lower concentrations of group D particles are preferable, even when compensated by a higher fluid velocity. However, concentrations of up to approximately 20% may still be feasible as both the minimum fluidisation velocity and mixing rate remain comparatively weakly affected by the presence of the larger particles.

Our main findings can be succinctly summarised as follows:

1. The addition of an increasing relative volume fraction of Geldart group D particles in a fluidised bed of group B particles increases the minimum fluidisation velocity in approximate agreement with the findings of Chiba et al. (1979).
2. The hydrodynamics in the fluidised bed are not significantly impacted until a point of critical loading of Geldart D particles on which a change in the flow patterns is observed. This flow pattern results in restricted and limited particle mixing (Windows-Yule et al., 2020).
3. Macro-mixing decreases linearly with increasing Geldart D concentration for low concentrations. the decrease in macro-mixing accelerates crossing a critical Geldart D loading. This suggests two main effects of Geldart D loading on the mixing:

(1) the presence of larger particles increases the solid–solid drag on tracer particles and (2) the alteration of the hydrodynamic flow pattern diminishes the overall ability of particles to move within the system.

4. Micro-mixing also decreases in the same fashion with rising Geldart D concentration indicating that the same mechanisms that affect macro-mixing also impede the mixing on a microscopic level.

Data availability

Data will be made available on request.

Declaration of Competing Interest

The authors declare that they have no known competing financial interests or personal relationships that could have appeared to influence the work reported in this paper.

Acknowledgements

The authors gratefully acknowledge support from EPSRC New Investigator Award EP/T034327/1, Royal Academy of Engineering Industrial Fellowship IF2021|89, Innovate UK KTP 11903, and Royal Society Grant RGS|R1|201054. Intensive computations required for this paper were performed using the University of Birmingham's BEAR Cloud service, which provides flexible resource for intensive computational work to the University's research community. See http://www.birmingham.ac.uk/bear for more details.

References

Bai, T., Sun, Z., Guo, Z., Zhu, J., Barghi, S., 2022. Bubble dynamics in a binary gas-solid fluidization system of geldart b and geldart d particles. Chem. Eng. Sci. 258, 117771.

Bokkers, G., van Sint Annaland, M., Kuipers, J., 2004. Mixing and segregation in a bidisperse gas–solid fluidised bed: a numerical and experimental study. Powder Technol. 140, 176–186. 1st International Workshop on Granulation (Granulation across the length scales: linking microscopic experiments and models to real process operation).

Chiba, S., Chiba, T., Nienow, A., Kobayashi, H., 1979. The minimum fluidisation velocity, bed expansion and pressure-drop profile of binary particle mixtures. Powder Technol. 22, 255–269.

Chiba, T., 1986. Prediction of the steady-state segregation patterns in gas fluidized beds with particles in throughflow. Fluidization, 185–192.

Edel, D., 2021. Uk's recycling technologies provides one bin solution for plastic waste. URL: https://www.intelligentliving.co/uks-recycling-technologies-provides-one-bin-solution-for-plastic-waste.

Formisani, B., Girimonte, R., 2003. Experimental analysis of the fluidization process of binary mixtures of solids. KONA Powder and Particle Journal 21, 66–75.

Gear, M., Sadhukhan, J., Thorpe, R., Clift, R., Seville, J., Keast, M., 2018. A life cycle assessment data analysis toolkit for the design of novel processes–a case study for a thermal cracking process for mixed plastic waste. Journal of cleaner production 180, 735–747.

Geldart, D., 1986. Gas fluidization technology. John Wiley and Sons Inc., New York, NY.

Gernon, T., Gilbertson, M., 2012. Segregation of particles in a tapered fluidized bed. Powder Technol. 231, 88–101.

Gilbertson, M., Eames, I., 2001. Segregation patterns in gas-fluidized systems. J. Fluid Mech. 433, 347–356.

Griffiths, A.E., 2020. Process and apparatus for treating waste comprising mixed plastic waste. US Patent 10,760,003.

Hameed, S., Sharma, A., Pareek, V., 2019. Modelling of particle segregation in fluidized beds. Powder Technol. 353, 202–218.

Huilin, L., Yurong, H., Gidaspow, D., Lidan, Y., Yukun, Q., 2003. Size segregation of binary mixture of solids in bubbling fluidized beds. Powder Technol. 134, 86–97.

Jena, H., Roy, G., Biswal, K., 2008. Studies on pressure drop and minimum fluidization velocity of gas–solid fluidization of homogeneous well-mixed ternary mixtures in un-promoted and promoted square bed. Chem. Eng. J. 145, 16–24.

Kim, D.Y., Lee, Y., Lee, J.K., Kim, S.D., Lee, D.H., et al., 2013. Takeover velocity in a gas-solid fluidized bed with binary solids.

Kunii, D., Levenspiel, O., 1991. Fluidization engineering. Butterworth-Heinemann.

Laverman, J., Fan, X., Ingram, A., van Sint Annaland, M., Parker, D., Seville, J., Kuipers, J., 2012. Experimental study on the influence of bed material on the scaling of solids circulation patterns in 3d bubbling gas–solid fluidized beds of glass and polyethylene using positron emission particle tracking. Powder Technol. 224, 297–305.

Leaper, M.C., Seville, J., Hilal, N., Kingman, S., Burbidge, A., 2004. Investigating the dynamics of segregation of high jetsam binary batch fluidised bed systems. Chem. Eng. Process. 43, 187–192.

Lun, C., Savage, S.B., Jeffrey, D., Chepurniy, N., 1984. Kinetic theories for granular flow: inelastic particles in couette flow and slightly inelastic particles in a general flowfield. Journal of fluid mechanics 140, 223–256.

Martin, T., Seville, J., Parker, D., 2007. A general method for quantifying dispersion in multiscale systems using trajectory analysis. Chemical engineering science 62, 3419–3428.

Nienow, A., Naimer, N., Chiba, T., 1987. Studies of segregation/mixing in fluidised beds of different size particles. Chem. Eng. Commun. 62, 53–66.

Nienow, A., NS, N., 1980. Continuous mixing of two particulate species of different density in a gas fluidised bed.

Nienow, A., Rowe, P., Cheung, L., 1978. The mixing/segregation behaviour of a dense powder with two sizes of a lighter one in a gas fluidised bed, in: Fluidization Proc. of the Second Eng. Found. Conf.", Trinity College, Cambridge, England, pp. 146–150.

Nienow, A.W., Edwards, M.F., Harnby, N., 1997. Mixing in the process industries. Butterworth-Heinemann.

Olaofe, O., Buist, K., Deen, N., Van der Hoef, M., Kuipers, J., 2013. Segregation dynamics in dense polydisperse gas-fluidized beds. Powder technology 246, 695–706.

Olivieri, G., Marzocchella, A., Salatino, P., 2004. Segregation of fluidized binary mixtures of granular solids. AIChE J. 50, 3095–3106.

Oschmann, T., Hold, J., Kruggel-Emden, H., 2014. Numerical investigation of mixing and orientation of non-spherical particles in a model type fluidized bed. Powder technology 258, 304–323.

Parker, D., Forster, R., Fowles, P., Takhar, P., 2002. Positron emission particle tracking using the new Birmingham positron camera. Nucl. Instrum. Methods Phys. Res., Sect. A 477, 540–545.

Rowe, P., Nienow, A., 1976. Particle mixing and segregation in gas fluidised beds. a review. Powder Technol. 15, 141–147.

Salatino, P., Solimene, R., 2017. Mixing and segregation in fluidized bed thermochemical conversion of biomass. Powder Technol. 316, 29–40.

Seville, J., Ingram, A., Parker, D., 2005. Probing processes using positrons. Chem. Eng. Res. Des. 83, 788–793.

Stein, M., Ding, Y., Seville, J., Parker, D., 2000. Solids motion in bubbling gas fluidised beds. Chem. Eng. Sci. 55, 5291–5300.

Taib, M.R., Kumoro, A.C., 2003. Effect of operating parameters on the minimum fluidisation velocity of an inclined fluidised bed. Jurnal Teknologi 38, 25–36.

Villermaux, J., 1986. Macro and micromixing phenomena in chemical reactors. Chemical Reactor Design and Technology. Springer, 191–244.

Wang, H., Yang, W., 2020. Application of electrical capacitance tomography in circulating fluidised beds–a review. Appl. Therm. Eng. 115311.

Wildman, R., Huntley, J., Hansen, J.P., Parker, D., Allen, D., 2000. Single-particle motion in three-dimensional vibrofluidized granular beds. Phys. Rev. E 62, 3826.

Windows-Yule, C., Gibson, S., Werner, D., Parker, D., Kokalova, T., Seville, J., 2020. Effect of distributor design on particle distribution in a binary fluidised bed. Powder Technol. 367, 1–9.

Windows-Yule, C., Moore, A., Wellard, C., Werner, D., Parker, D., Seville, J., 2020. Particle distributions in binary gas-fluidised beds: Shape matters–but not much. Chem. Eng. Sci. 216, 115440.

Windows-Yule, C., Parker, D., 2014. Self-diffusion, local clustering and global segregation in binary granular systems: The role of system geometry. Powder technology 261, 133–142.

Windows-Yule, C., Seville, J., Ingram, A., Parker, D., 2020. Positron emission particle tracking of granular flows. Annual review of chemical and biomolecular engineering 11, 367–396.

Windows-Yule, C., Weinhart, T., Parker, D., Thornton, A., 2014. Effects of packing density on the segregative behaviors of granular systems. Physical review letters 112, 098001.

Windows-Yule, C.R., Herald, M., Nicusan, L., Wiggins, C., Pratx, G., Manger, S., Odo, E., Leadbeater, T., Pellico, J., de Rosales, R., et al., 2021. Recent advances in positron emission particle tracking: a comparative review. Rep. Prog. Phys.

Windows-Yule, K., Nicuşan, L., Herald, M.T., Manger, S., Parker, D., 2022. Positron emission particle tracking.

Wu, S., Baeyens, J., 1998. Segregation by size difference in gas fluidized beds. Powder Technol. 98, 139–150.

Zhang, W., Wang, C., Yang, W., Wang, C.H., 2014. Application of electrical capacitance tomography in particulate process measurement–a review. Adv. Powder Technol. 25, 174–188.